Proceedings of the Sixth International Conference on
Railway Technology: Research, Development and Maintenance
Edited by: J. Pombo
Civil-Comp Conferences, Volume 7, Paper 3.21
Civil-Comp Press, Edinburgh, United Kingdom, 2024
ISSN: 2753-3239, doi: 10.4203/ccc.7.3.21

Influence of Strong Wind on the Aerodynamic Characteristics of the High-Speed Maglev Train

J. Sun[1,2], M.-Z. Yang[1], L. Zhang[1], W.-X. Teng[3] and G. Chen[2]

[1]School of Traffic & Transportation Engineering, Central South University, Changsha, China
[2]Aerodynamics Research Group, CRRC CHANGCHUN GERMANY RailTech GmbH, Aachen, Germany
[3]Railway Vehicle System Integration Laboratory, CRRC Changchun Railway Vehicles Co., Ltd, ChangChun, China

Abstract

The increasing demand for high-speed transportation has led to the successive development and building of high-speed maglev transportation systems by Germany, Japan, the United States, and China. Though the design speed of the high-speed maglev train has been increased to 600 km/h, however, the degree of deterioration of their aerodynamic characteristics under strong winds has not been studied because of its high speed and different operation modes compared to wheel rail trains. In this study, the delayed detached eddy simulation method is used to simulate the flow field around the maglev train under strong wind, and the characteristics of flow field around the maglev train and the influence of aerodynamic force on the maglev train under different wind conditions are studied. The results show that with the deterioration of the wind condition, the drag, lift and side force of the head car and tail car of the maglev train change. Furthermore, an increase in strong winds causes the flow field asymmetry and vortex intensity around the train to increase, resulting in further fluctuations of the aerodynamic characteristics of the train.

Keywords: strong wind, maglev train, aerodynamic characteristics, high speed train, flow structures, delayed detached eddy simulation.

1 Introduction

For a traditional high-speed wheel rail train, when the speed reaches a certain value, the wheel rail adhesion coefficient decreases rapidly with the increase of the train speed, which may lead to the traction power decrease, wheelset slip, and vehicle

instability. Therefore, it is difficult for the traditional wheel rail high-speed train to ensure the stability and safety of continuous high-speed operation above 500 km/h [1]. Thus, to further improve the running speed of trains, Germany, Japan, and China have successively developed their own high-speed maglev transportation systems. The difference between the maglev and traditional wheel rail trains is that the maglev system keeps the train floating through repulsive or attractive forces between magnetic poles to realize contactless operation and thereby reduces the friction between the train and track, which enables running speeds up to 600km/h [2]. However, such high-speed maglev trains suffer from certain problems, such as the rapid increase in air resistance, surge in transient pressure caused by tunnels, and sharp deterioration of train aerodynamic performance caused by the crosswind. With the increase of maglev train speed, the flow field around the train becomes more and more complex [3]. Among the factors affecting the safe operation of high-speed trains, strong wind is a key parameter [4]. In 2007, strong winds overturned 11 carriages on the South Xinjiang line, causing heavy property losses and seriously endangering the lives of passengers. Therefore, a strong wind environment directly affects the safe operation of trains [5]. However, research on the aerodynamic performance of high-speed maglev trains with speeds of more than 600 km/h in a crosswind environment is relatively lacking. Therefore, in order to evaluate the safety of the normal maglev train in the strong wind environment, it is necessary to study the evolution of the flow field around the high-speed maglev train and the variation of the aerodynamic force of the train under the strong wind.

Previous studies on the aerodynamic impact of strong wind on train mainly focus on wheel rail train. Strong wind will increase the fluctuation of flow field around the train, worsen the aerodynamic performance of high-speed train, and easily cause shaking and even overturning of high-speed train [6]. Chen studied the influence of train shape parameters under crosswind. The results show that the sensitivity of aerodynamic force of high-speed train increases under crosswind, i.e., the change of train shape parameters under cross wind makes the amplitude of aerodynamic force greater than that without crosswind[7]. Hemida used LES method to study the aerodynamic performance of freight cars under crosswind and considered that crosswind would lead to the deterioration of flow field structure and aerodynamic performance around freight cars[8]. Jiqiang experimentally studied the influence of scale on the aerodynamic performance of high-speed train with or without crosswind[9]. It is considered that crosswind aggravates the influence of scale on the drag coefficient of the head car, and increasing scale will reduce other force coefficients.

The maglev train is similar to the high-speed train running on the viaduct. Ming believe that in comparison with the flat ground, the aerodynamic performance of high-speed train running on viaduct under crosswind condition will be worse[10]. He studied the aerodynamic characteristics of high-speed train on viaduct under crosswind and showed that the track position has an impact on them. Compared with the windward side, the pressure fluctuation of leeward train is obviously disturbed by the track[11]. E D studied the aerodynamic performance of high-speed train running from a tunnel to a bridge or entering a tunnel from a bridge under crosswind conditions. It was found that the amplitude of the force coefficient changes more

during the process of entering the tunnel from the bridge, and the aerodynamic fluctuation amplitude from the bridge to the tunnel is larger than that from the tunnel to the bridge[12]. Though there has been a significant improvement in the speed of high-speed maglev trains, the coupling effect of train speed and wind speed on the flow field and aerodynamic force around the train has not been studied. Therefore, it is necessary to simulate and analyze the aerodynamic characteristics of high-speed maglev trains running on high bridges under crosswinds.

At present, only a few studies on the influence of strong winds on the flow field structure evolution mechanism and aerodynamic performance of high-speed maglev trains exist. The flow mechanism and aerodynamic performance degradation effect of the flow field around the high-speed maglev train when its speed reaches to 600 km/h have not yet been studied. The differences and similarities of fine structures in the flow field and aerodynamic forces around the high-speed maglev train have not been published. In this study, an aerodynamic simulation model of the normal maglev system has been established, and the aerodynamic force and the surrounding flow field of the maglev train under the action of different crosswind speeds were studied via the delayed detached eddy simulation (DDES) method. The distribution of pressure and vortex structure on the windward and leeward sides of the train under different wind conditions were compared and analyzed, and the influence mechanism of strong wind parameters on the flow field structure evolution mechanism and aerodynamic characteristics around the high-speed maglev train has been clarified.

2 Numerical method

2.1 Methodology

According to the results of Hemida[13], large eddy simulation (LES) is effective to simulate the flow field around high-speed train. However, it requires a large number of grids to ensure accuracy, especially near the train surface area. Considering grid density, the Reynolds-averaged Navier-Stokes (RANS) model requires a lower grid density than LES; however, RANS causes difficulties in simulating unsteady flow field accurately. In contrast, detached eddy simulation (DES) combines the advantages of LES and RANS. The DES method uses RANS to simulate the flow field near the train surface and LES to simulate the flow field far away from the train surface, this combination method can reduce the number of grids near the train. However, DES also has high grid requirements. When the Reynolds number is very high, the distorted grid and the wrong position of the interface between RANS and LES lead to inaccurate calculations, resulting in a decrease in eddy viscosity and the stress depletion effect of the model. To overcome this, many scholars use the DDES method to simulate and delay the change between RANS and LES [14]. Therefore, in this study, the DDES method was used to simulate the flow field around the train.

Further, the STAR-CCM+ software based on a finite volume solver was used to simulate the flow field structure around the train. The train speed was 600 km/h, and the Mach number was approximately 0.49; thus, the fluid was a compressible viscous fluid. Addition, to achieve effective accuracy, space and time discretization was adopted, thereby achieving two orders. The time step was set to 2×10^{-4} s, which can

capture both the mainstream and the vortex formed and separated by the maglev train sheath and track.

2.2 Details of computational models

The wind yaw angle β is defined as the angle between the wind speed and composite wind speed (combination of driving and crosswind speeds) in the opposite direction of train operation, which reflects the coupling relationship between train speed and ambient wind speed. The definitions of the resultant wind and wind angle are presented in Fig.1.

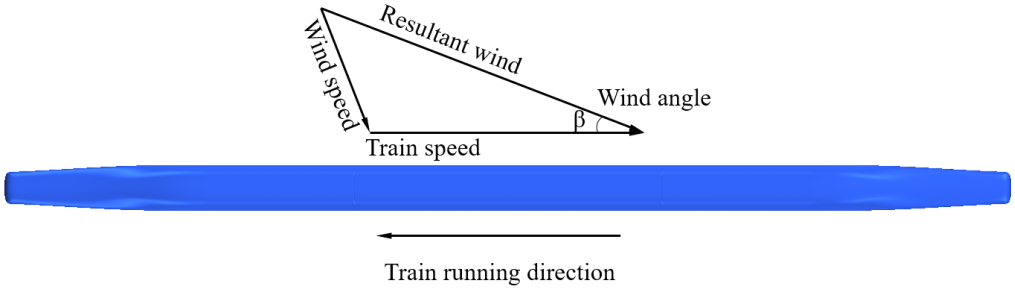

Figure 1: Definition of resultant wind and wind angle β.

To analyze the aerodynamic performance of the normal maglev train under crosswind, a 3-D model of the normal maglev train was established, with the model scale being 1:1. The size of the train is shown in Fig. 2. The train comprised of three cars. The parameters of the train were dimensionless, based on the height from the bottom of the track to the roof of the maglev train. The height, H, was 4.2 m; length of the head and tail cars of the maglev train were 6.15 H each; length of the middle car was 5.28 H; width and height of the train were 0.81 H and 0.92 H, respectively.

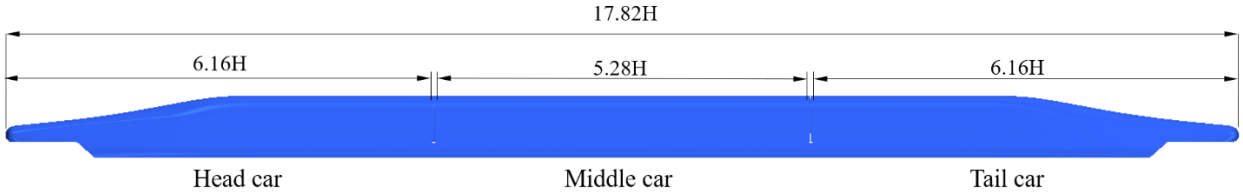

(a)

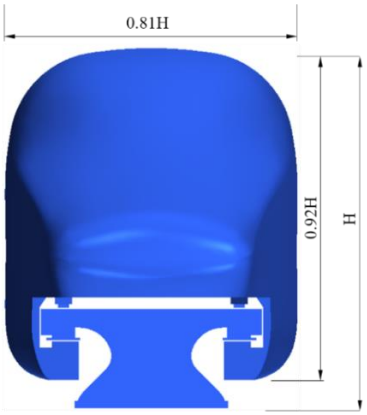

(b)

Figure 2: Model of the normal maglev train: (a) side view and (b) front view.

To obtain the aerodynamic influence of the crosswind speed on the normal maglev train, we considered five scenarios, the maglev train running speed was 600 km/h, and the corresponding crosswind speeds were 0, 12, 15, 19, 22, and 26 m/s, respectively (see Table 1).

Train speed [km/h]	Wind speed [m/s]	Wind speed class	Wind angle [°]
600	0	0	90
	12	6	
	15	7	
	19	8	
	22	9	
	26	10	

Table 1: Computational conditions.

2.3 Computational domain and boundary conditions

The size and boundary conditions of the computational domain are illustrated in Fig. 3. For comparison, the computational domain is made dimensionless according to the height from the bottom of the maglev train rail to the top of the maglev train. The width and length of the computational domain should satisfy the full development of the train's lateral flow field and wake vortex flow under the action of a crosswind. According to the research of Jiqiang [15], the length of computational domain AB is taken to be 46.2H, and the width of windward side is 13.2H. Considering the complex flow field structure of leeward side, the width of leeward side is 33H, which is 2.5 times of the windward side. The boundary conditions of planes ABCD and $BCC'B'$ are defined as the velocity inlet boundary conditions, and the velocity is the combined velocity of wind speed and the maglev train speed; the distance between ABCD surface and nose of the head car is 22H. The boundary conditions of plane $A'B'C'D'$ and plane $ADD'A'$ are defined as pressure outlet, and the reference pressure is 0 Pa. The distance between plane $A'B'C'D'$and nose of the tail car is 71H, which is 3.2 times of that between plane ABCD and nose of the head car. The height of calculation domain is 17.6H.

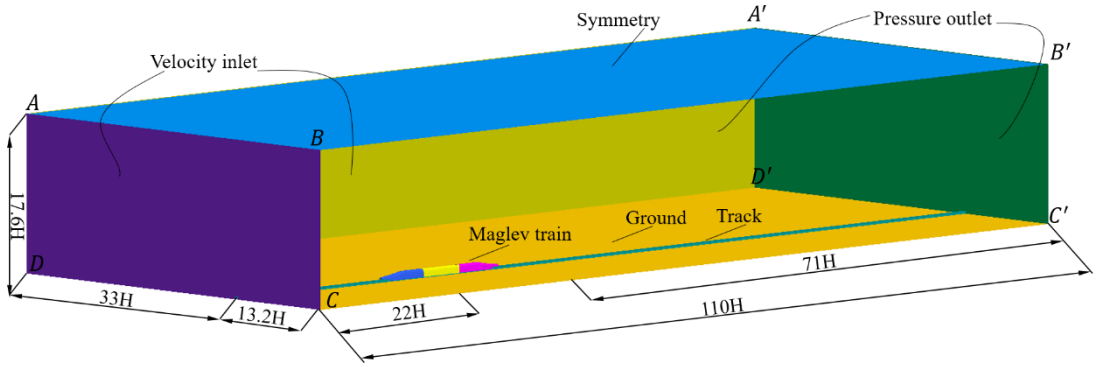

Figure 3: Computational domain and boundary conditions.

2.4 Grid generation

The simulation quality of DDES is highly dependent on the grid resolution because the switching between URANS and LES is largely affected by the size of the grid and the solver ability. The solver ability determines whether the LES region can analyze the small-scale flow structure according to the size of the grid. The computational domain grid was generated by STAR-CCM+, with the trim grid type. To capture the small-scale vortex structure in the flow field, surface control was carried out in the car body, track, tail car, and other areas. Thereafter, 4 encryption areas were set around the train for local encryption, the closer the encryption area was to the train, the denser the grid. To accurately simulate the flow of the train body area and capture the development process of the body along the wall to the external space area, a 20-prism layer grid was used in the train wall area. The 20-prism layer was added to the train surface. The thickness of the first layer grid was 0.164 mm and the growth rate was 1.2, which is consistent with the recommendation of the STAR-CCM+ user guide that the growth rate used should be less than 1.5. Because the full y+ wall function was adopted, the average y+ of the first layer grid attached to the train surface was approximately 30. However, as the flow away from the body was not sufficient to affect the flow around the train, the grid size away from the body was larger. When the grid transits from the encrypted region to a region far away from the flow core, the grid between each encrypted region was set to grow slowly.

To clarify the grid fineness, the independence of the grid in the computational domain is firstly studied. Considering the running speed of the maglev train as 600 km/h coupled with crosswind speed of 26 m/s condition, the aerodynamic variation of the high-speed maglev train was simulated under three sets of grids with different fineness: coarse, medium, and fine grids numbering at 34.75, 43.56, and 54.84 million respectively. The flow field structure around the train for the three different grid sizes is shown in Fig. 4.

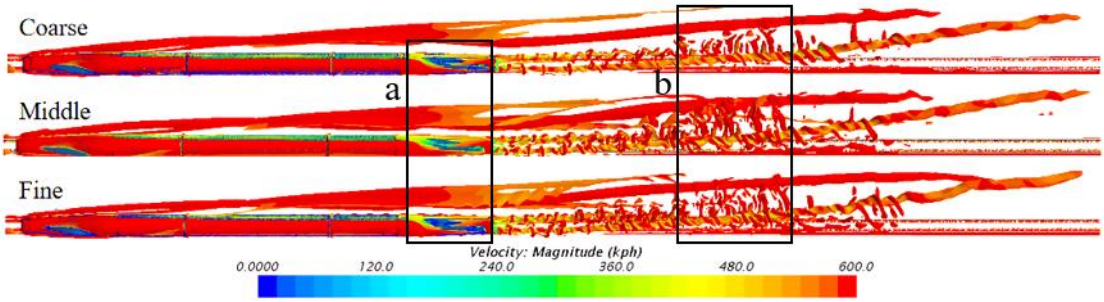

Figure 4: Vortex structures around the train with different grid sizes (Top view) (Q=200).

The flow field structure around the high-speed maglev train with different grid sizes shows that the vortex around the maglev train is determined by the grid density to a certain extent, specifically in the rear areas ‘a’ and ‘b’ of the maglev train. With an increase in grid density, the structure of the wake vortex obtained via the medium and fine grid simulations was similar. To further illustrate the influence of the grid size on the aerodynamic force of the train, the drag, side, and lift coefficients of its head, middle, and tail cars under three different grid sizes were compared and analyzed, as shown in Table 2.

Case	Mesh number [Million]	C_d			C_s			C_l		
		Head car	Middle car	Tail car	Head car	Middle car	Tail car	Head car	Middle car	Tail car
Coarse	3.8	0.056	0.096	0.159	0.381	0.094	0.162	1.386	0.999	0.712
Medium	4.4	0.056	0.095	0.155	0.394	0.092	0.161	1.394	0.946	0.664
Fine	5.5	0.057	0.096	0.152	0.395	0.093	0.165	1.384	1.040	0.695

Table 2: Grid number and aerodynamic coefficient.

It is evident from Table 2 that the force coefficients obtained from the three diffrent grid sizes are similar. Furthermore, the error calculations are based on the calculation results of the fine grid. Using Equation (1), the maximum change in various coefficients is 5.30 %; according to Yuangui [16], it meets the accuracy requirements of this calculation. In particular, the maximum difference between the medium and fine grids was less than 4.46 %. Considering the consistency of the flow field structure around the high-speed maglev train under the two grid-scale conditions, we study the medium grid dispersion method to improve the calculation efficiency. Thus, the grid size of the discrete maglev train is 43.56 million. Some of the grids used in the numerical calculations are shown in Fig. 5.

$$e = \frac{\left| C_{coarse} - C_{fine} \right|}{C_{fine}} \tag{1}$$

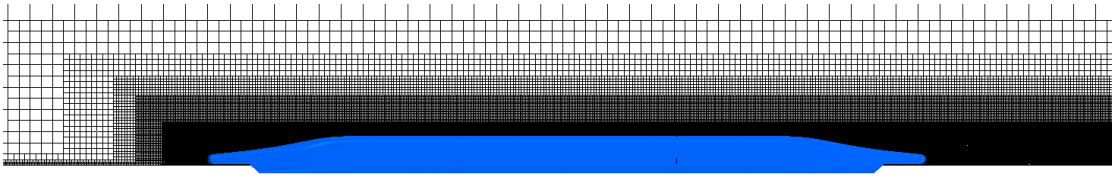

(a)

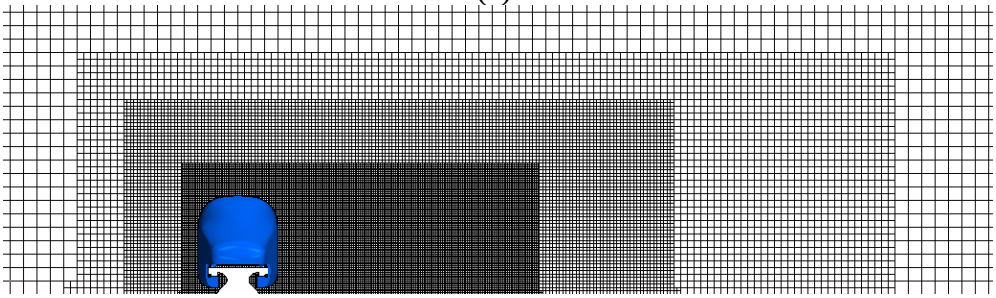

(b)

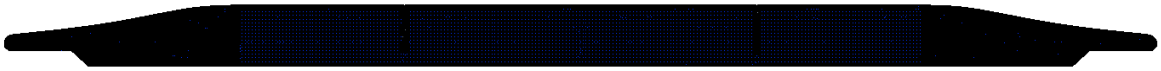

(c)

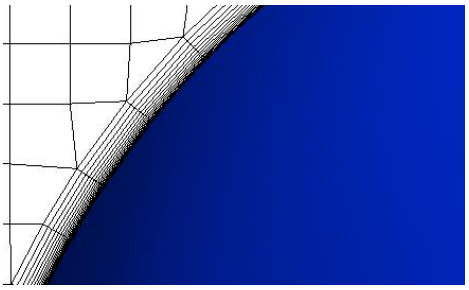

(d)

Figure 5: Grid of maglev train: (a) side view, (b) front view, (c) maglev train surface mesh, and (d) 20-prism layer.

2.5. Dimensionless coefficients

Equations (2) and (3) give the pressure and speed coefficients, respectively; where p_0 is the average static pressure; reference pressure p_0 is 0 Pa; air density ρ is 1.225 kg/m^3; V_0 is the resultant wind speed.

$$C_P = \frac{p - p_0}{0.5\rho V_0^2} \quad (2)$$

For analysis, the aerodynamic coefficients were standardized before comparison as follows:

$$C_D = \frac{D}{0.5\rho V_0^2 S_0} \quad (3)$$

$$C_L = \frac{L}{0.5\rho V_0^2 S_0} \quad (4)$$

$$C_S = \frac{S}{0.5\rho V_0^2 S_0} \quad (5)$$

D, L ,and S are defined as the drag, lift, and side force, respectively; C_D, C_L, and C_S are defined as the drag, lift, and side force coefficients, respectively. S_0 is the reference area , ρ is the air density.

3 Results

3.1 Validation of numerical simulation results

To ensure the reliability of the calculation method, the wind tunnel test results were used for verification. Further, to verify the accuracy of the numerical calculation results, a numerical simulation model was constructed according to the relevant size parameters in the wind tunnel test. A comparison between the numerical simulation results and the wind tunnel test results is presented in Table 5.

Drag coefficients	Head car	Middle car	Tail car
Test	0.080	0.101	0.097
Simulation	0.082	0.097	0.103
Deviation[Hz]	2.4	4.1	5.8

Table 3: Algorithm validation.

The results of the wind tunnel test and numerical simulation show that the maximum difference between the test and the simulation values is 5.8 %, which verifies the credibility of the numerical simulation method.

3.2 Comparison of flow structure

To further understand the flow field structure around the high-speed maglev train under strong winds, in this study, we primarily analyze the development and evolution of eddy currents around the train. Thereafter, we use the Q criterion to determine the computational domain vortex, which is the second invariance of the velocity gradient. Q is defined as follows:

$$Q = -\frac{1}{2}\left(||S||^2 - ||\Omega||^2\right) = -\frac{1}{2}\left(\left(\frac{\partial \overline{u_i}}{\partial \overline{x_i}}\right)^2 - \frac{\partial \overline{u_i}\partial \overline{u_j}}{\partial \overline{x_i}\partial \overline{x_j}}\right) = \frac{1}{2}\frac{\partial \overline{u_i}\partial \overline{u_j}}{\partial \overline{x_i}\partial \overline{x_j}} \qquad (6)$$

where u_i, u_j are the velocity component under the cartesian coordinate system, S is the rate strain tensor of the velocity variable, and Ω is the rotation rate tensor of the velocity variable. An ISO with a positive value of Q shows the dominant position strain in the fluid and indicates the vertical structure in the flow[17].

According to the definition of Q, the ISO is established with Q = 200. In order to analyze the influence of the change of crosswind velocity on the flow field around the maglev train, the transient flow field structure around it was analyzed. When the train is running at high speed, the flow field around the train is very complex and contains all kinds of fluctuating vortex structures, especially the flow field at the rear of the tail car. These vortices are generated by the streamlines of the head and the tail car, and continue to develop to the rear of the train. In the absence of strong wind, the vortex structure at the rear of the train is relatively symmetrical. Moreover, when the train is affected by strong wind, the vortex structure deflects to the leeward side, showing asymmetry.

Fig. 6 shows the top view of the train with a vortex structure corresponding to different crosswind speeds, wherein the background color indicates the velocity of the flow field around the train. The vortex structure is colored by normalized velocity, which is defined as follows:

$$U_{GF} = \frac{U_\infty - U_{TF}}{U_\infty} \qquad (8)$$

$$V_{GF} = \frac{V_{TF}}{U_\infty} \qquad (9)$$

$$W_{GF} = \frac{W_{TF}}{U_\infty} \qquad (10)$$

$$U_{Slipstream} = \sqrt{U_{GF}^2 + V_{GF}^2 + W_{GF}^2} \qquad (11)$$

U_{TF}, V_{TF}, and W_{TF} represent the speeds in X, Y and Z directions based on the fixed coordinate system of the train, which can be obtained directly through simulation. GF and TF represent the ground reference system and train reference system respectively.

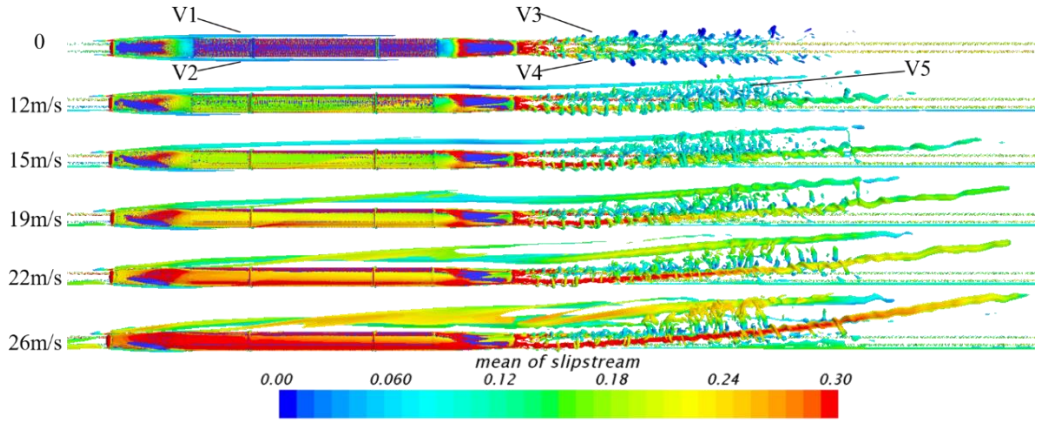

Figure 6: Vortex structures around the train with the different winds (Top view) (Q=200).

According to the vorticity shown in Figs. 6, it can be divided into five main vortex structures according to the source. Vortices V_1 and V_2 develop from the head of the normal maglev train and move backward. With an increase in the crosswind speed, vortex V_1 develops further away from the vehicle body and finally develops into the tail flow area of the train in a spiral manner, while V_2 was produced on the windward side of the train without the influence of wind. With the negative impact of the environment wind, vortex V_2 decreases until it is close to the car body. In contrast, vortices V_3 and V_4 were generated at the rear of the train. In the case of strong wind, V_5 is separated from the periphery of V_4, and V_4 develops to the leeward side. When the strong wind environment is worse, the strength of V_4 core is more obvious. In the absence of wind, the vortices V_3 and V_4 show strong symmetry, while V_5 does not. In the region far from the rear of the train, V_4 has a vortex core and a high speed. V_1, V_3, V_4, and V_5 gradually merge with each other, enhancing the coupling effect, thereby increasing the strength of the vortices. In particular, the rail surface coupling of V_4 and V_5 at the rear of the train. As far as the abundance of vortices at the tail of maglev train is concerned, the abundance of small vortices V_5 between V_3 and V_4 caused by sidewind is higher than that caused by crosswind.

3.3 Comparison of aerodynamic pressure coefficients

The train surface pressure directly affects the aerodynamic performance of the train. Therefore, it is important to compare and analyze the changes in the surface pressure of the maglev train under different wind conditions. The mean pressure distribution on the train surface is shown in Figure 7.

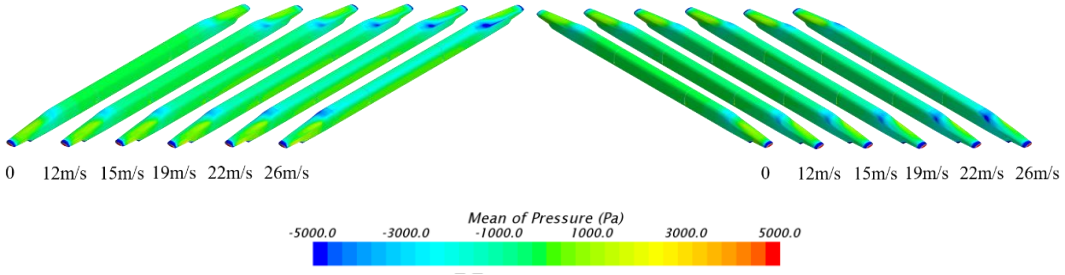

(a) (b)

Figure 7: Mean pressure distribution on the maglev train:(a) windward of crosswind, (b) leeward of crosswind.

Figure 7 shows that with the enhancement of strong wind characteristics, the pressure change on the surface of the maglev train follows a relatively consistent law: with the enhancement of wind effect, the positive pressure coefficient on the windward side of the streamline of the head train increases. There is a weak negative pressure at the transition between streamline and non-streamline in the head car. With the increase of wind speed, the negative pressure in this area also increases, and it begins to move to the leeward side. There is a large negative pressure at the transition between streamline and non-streamline in the tail of the maglev train. With the increase of wind intensity, the negative pressure value and area on the windward side also increase. The positive pressure appears on the leeward side of the tail car. With the increase of the wind intensity, the positive pressure value and the positive pressure range remian unchanged. For the non-streamline region, the pressure value does not change with the change of wind. In order to analyze the surface pressure distribution of the maglev train more precisely, the surface pressure value of the maglev train is taken at the 0.357H horizontal line of the maglev train height, which passes through the nose of the maglev train. The pressure value of the maglev train on the horizontal line is shown in Fig. 8.

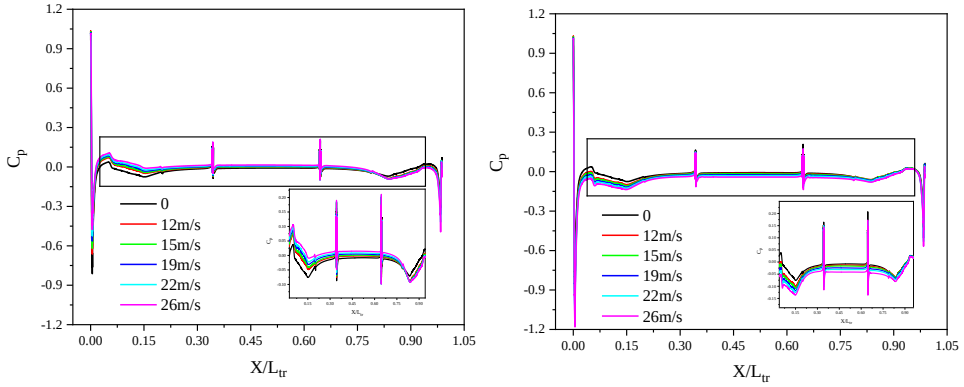

(a) (b)

Figure 8: Pressure coefficient of the maglev train under the crosswind condition: (a) windward side and (b) leeward side.

Fig. 8 (a) depicts the pressure coefficient on the windward side of the maglev train under crosswind. It shows that when the crosswind speed reaches 19 m/s, the pressure in the non-streamline area of the maglev train is 0 Pa; and with the increase of crosswind speed, the pressure in this region also increases. Thereafter, due to the change of the maglev train shape, the pressure coefficient of the streamlines of the head and tail cars, inter-carriage gap area and changes dramatically. Further, the pressure coefficients of the head, middle, and non-streamline area of the tail car increase with the increase in the crosswind speed. The pressure coefficient of the streamline area of the tail car decreases with the increase of the crosswind speed. Under the condition of no wind, the streamline pressure coefficient of the tail car is larger than that under the condition of wind, but under the condition of wind, the streamline pressure coefficient of tail car does not change significantly. Fig.8 (b) shows the pressure coefficient on the leeward side of the maglev train under crosswind. In this study, the pressure coefficient of maglev train is in the negative pressure area, and the non-streamline area of the maglev train pressure coefficient continues to decrease. In the streamline region of the tail car, the pressure coefficient is almost unchanged in both windy and windless conditions, which is different from the windward side.

Pressure variation law of the inter-carriage gap area: The pressure variation of the maglev train is very severe; with the increase of crosswind speed, the pressure in the windward at the inter-carriage gap area increases, while the pressure in the leeward side decreases.

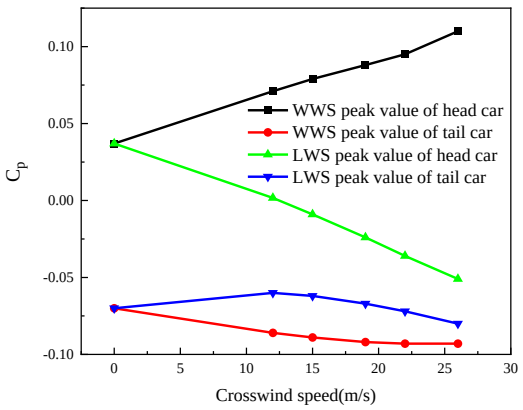

Figure 9: Peak pressure coefficient.

In order to further understand the change law of pressure coefficient on the horizontal line at 0.357H, Fig. 9 shows the curve of the peak pressure on the windward side and leeward side of the maglev train with the crosswind speed. For the head car, when the crosswind speed increases from 12 m/s to 26 m/s, the peak value of positive pressure coefficient on the windward side increases linearly, and the peak value of pressure coefficient increases by 0.039. The peak value of negative pressure coefficient on the leeward side is linearly decreasing, and the absolute value of negative pressure

coefficient increases by 0.088. For tail car, the pressure coefficient peak changes on the windward side and the leeward side are not as obvious as that of the head car, and the absolute of the peak values of the pressure coefficients on the windward and the leeward sides increase by 0.023 and 0.02 respectively.

3.4 Comparison of aerodynamic force coefficients

To determine the influence of the flow field vortex structure and maglev train surface pressure on the aerodynamic force of each car, the drag coefficient of each car under strong wind conditions is shown in Fig. 10. Fig. 10 shows that with the increase of wind disturbance, the drag coefficient of the head car decreases, and that of the tail car increases, while the drag coefficient of the middle car remains unchanged.

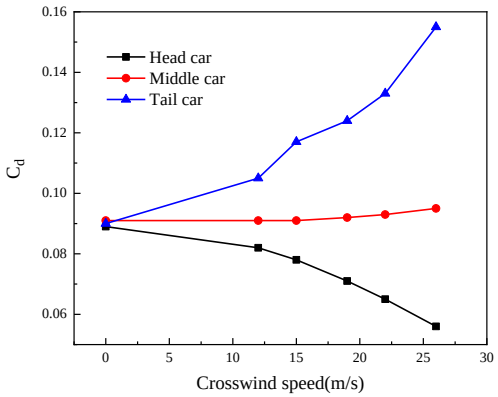

Figure 10: Drag force coefficient.

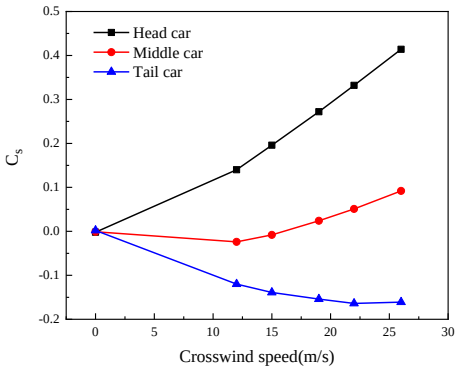

Figure 11: Side force coefficient.

Fig. 11 shows the side force coefficient under strong wind, in which the side force coefficient of the head car is the largest, the side force coefficient of the middle car is the smallest, and the side force coefficient of the tail car is opposite to that of the head car and the middle car. It can be seen from Section 3.3 that with the increase of wind, positive pressure is formed on the windward side of the train, while vortex separation occurs on the leeward side, and the negative pressure increases continuously, resulting in the increase of the side force coefficient of the head car. Because the pressure distribution law of the tail car is opposite to that of the head car, the absolute value of the side force coefficient of the tail car increases. In addition, for the middle compartment, the wind has little effect on the pressure on the windward side and leeward side.Therefore, the sensitivity is weaker than that of the head and the tail car. Under the action of crosswind, the coefficient of train side force increases linearly.

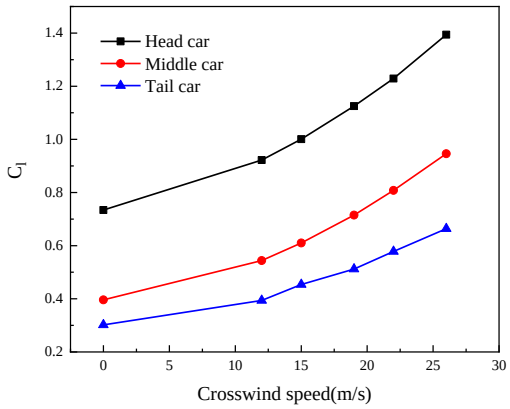

Figure 12: Lift force coefficient.

Fig.12 shows the lift coefficient under strong wind, in which the lift coefficient of the head car of maglev train is the largest and that of the tail car is the smallest. When the crosswind speed is greater than 15 m/s ,the lift of the maglev train is greater than 1, which indicates that the bad wind environment has a great impact on the safety of the maglev train. Similarly, with the increase of crosswind speed, the lift of the three cars of the maglev train increases linearly.

4 Conclusions and Contributions

In this study, the aerodynamic performance of a maglev train under strong winds was studied. The flow field structure, surface pressure, and aerodynamic force of a high-speed maglev train under crosswind and sidewind were compared and analyzed. The specific conclusions are as follows:

(1) Under strong winds, there are five main vortices around the train. With the strengthening of the wind, the vortex structure on the leeward side of the head train becomes wider and longer, while the spiral shedding and interaction coupling effect of the two vortices in the wake become stronger. With the increase of wind, the number of small vortices separated from the windward side of the tail car is greater.

(2) With the increase of crosswind wind speed, the pressure on the train surface begins to change. Positive pressure appears on the windward side of the head car, and negative pressure appears on the leeward side of the head car. The pressure distribution of the tail car and the head car is opposite. The peak pressure analysis of the head and tail cars of the maglev train shows that the response intensity of the head car to the external wind environment is stronger than that of the tail car.

(3) The variation of the three force coefficients is consistent, the force coefficient increases linearly with the increase of crosswind speed. The side force and lift directly affect the safe operation of the maglev train and the wind environment is more sensitive to the change of the lift of the maglev train. When the crosswind speed reach 15 m/s, the lift coefficient of the maglev train head car can reach 1.

Acknowledgements

The authors would like thank CRRC Changchun Railway Vehicles Co.,ltd, CRRC CHANGCHUN GERMANY RailTech GmbH, School of Traffic & Transportation Engineering, Central South University.

References

[1] Wu, B., Wu, Z.F., Wang, H.Y., Jin, X.S., 2013. Study on factors affecting high-speed wheel rail adhesion characteristics. J. China Railw Soc. 3, 18–22.
[2] Hyung-Woo Lee, Ki-Chan Kim, Ju Lee, 2006. Review of maglev train technologies. IEEE Trans. Magn. 42, 1917–1925.
[3] Raghunathan, R.S., Kim, H.-D., Setoguchi, T., 2002. Aerodynamics of high-speed railway train. J. Progr. Aeosp Sci. 38, 469–514.
[4] Tian, H., 2010. Research progress in railway safety under strong wind condition in China. J. Cent. S. Univ. 41, 2435–2443.
[5] Lei, Z., Ming-zhi, Y., Xi-feng, L., 2018. Experimental study on the effect of wind angles on pressure distribution of train streamlined zone and train aerodynamic forces. J. Wind Eng. Ind. Aerod. 174, 330–343.
[6] Baker, C.J., 2009. The effect of unsteady crosswind forces on train dynamic be haviour, in: Proceedings of the 5th European and African Conference on Wind Engineering, Florence, Italy.
[7] Chen, Z., Liu, T., Jiang, Z., Guo, Z., Zhang, J., 2018. Comparative analysis of the effect of different nose lengths on train aerodynamic performance under crosswind. J. Fluids Struct. 78, 69–85.
[8] Hemida, H., Baker, C.J., Gao, G., 2014. The calculation of train slipstreams using large-eddy simulation. Proc. Inst. Mech. Eng. F. 228, 25–36.
[9] Jiqiang, N., Xifeng, L., Dan, Z., 2016. Experimental study on the effect of Reynolds number on aerodynamic performance of high-speed train with and without yaw angle. J. Wind Eng. Ind. Aerod. 157, 36–46.
[10] Ming, W., Xiaozhen, L., Jun, X., Qiyang, Z., Haiqing, S., 2018. An experimental analysis of the aerodynamic characteristics of a high-speed train on a bridge under crosswinds. J. Wind Eng. Ind. Aerod. 177, 92–100.
[11] He, X., Zuo, T., Zou, Y., Yan, L., Tang, L., 2020. Experimental study on aerodynamic characteristics of a high-speed train on viaducts in turbulent crosswinds. J. Cent. S. Univ. 27, 2465–2478.
[12] E, D, Weichao, Y., Xuhui, H., Yichao, Y., Zhihui, Z., Ang, W., 2020. Transient Aerodynamic Performance of High-Speed Trains When Passing Through an Infrastructure Consisting of Tunnel–Bridge–Tunnel Under Crosswind. Tunn, J. Undergr. Space Technol. 102. 103440.
[13] Hemida, H., Baker, C.J., Gao, G., 2014. The calculation of train slipstreams using large-eddy simulation. Proc. Inst. Mech. Eng. F. 228, 25–36.
[14] Zhang, J., Li, J., Tian, H., Gao, G., Sheridan, J., 2016. Impact of ground and wheel boundary conditions on numerical simulation of the high-speed train aerodynamic performance. J. Fluids Struct. 61, 249–261.
[15] Jiqiang, N., Dan, Z., Yueming, W., 2018. Numerical comparison of aerodynamic performance of stationary and moving trains with or without windbreak wall under crosswind. J. Wind Eng. Ind. Aerod. 182, 1–15.

[16] Yuangui, M., Hanbing, Z., Dawei, C., Yonggang, Y., 2020. Numerical simulation of initial compression wave characteristics of 600 km·h−1 maglev train entering tunnel. J. Traffic Transp. Eng. 20, 120–131.
[17] Jeong, J., Hussain, F., 1995. On the identification of a vortex. J. Fluid Mech. 285, 69–94.